R. & M. No. 2800
(13,768)
(A.R.C. Technical Report)

MINISTRY OF SUPPLY

AERONAUTICAL RESEARCH COUNCIL
REPORTS AND MEMORANDA

Wind-tunnel Tests on Two-dimensional Supersonic Aerofoils at M = 1·86 and M = 2·48

By

D. BEASTALL, B.Sc., and R. J. PALLANT

LONDON: HER MAJESTY'S STATIONERY OFFICE

1954

PRICE 5*s*. 6*d* NET

Wind-Tunnel Tests on Two-Dimensional Supersonic Aerofoils at M = 1·86 and M = 2·48

By

D. BEASTALL, B.Sc., and R. J. PALLANT

COMMUNICATED BY THE PRINCIPAL DIRECTOR OF SCIENTIFIC RESEARCH (AIR), MINISTRY OF SUPPLY

Reports and Memoranda No. 2800*

July, 1950

Summary.—Wind-tunnel tests, at Mach numbers 1·86 and 2·48, have been carried out on two-dimensional unswept double-wedge and circular-arc aerofoils to study the viscous effects which are not accounted for in the linearised and shock-expansion aerofoil theories. The aerofoil characteristics derived from the measured surface pressures are compared with the theoretical values.

Schlieren observation was employed to examine the flow and, in particular, the separation near the trailing edges of the aerofoils. In an appendix the results obtained from experiments on breakaway caused by a step on a flat plate[1,2] are applied to the aerofoil tests as a method of assessing the pressures in the dead-water regions formed by the flow separation, and comparison is made with the measured pressures.

Disturbing the boundary layer by means of wires caused a delay in separation; pitot-tube traverses through the boundary layers with and without wires illustrated the change in velocity profile between the two cases. The position of separation was briefly examined also by the use of oil; the point of separation as indicated by this method was in fair agreement with that given by pressure measurements, for cases of considerable separation only.

1. *Introduction.*—The linearised supersonic aerofoil theory assumes air to be an inviscid fluid and all perturbation velocities to be small; the shock-expansion theory neglects viscosity but takes into account the shock-waves at the leading and trailing edges. Two-dimensional aerofoil characteristics can easily be derived on these assumptions, but the validity of the results will depend to a large extent on the magnitude of the viscous effects. These effects can be divided into two main parts, the skin friction forces, and the changes in the flow configuration caused by the flow separation from the solid boundaries. It is the purpose of this report to examine the effects due to flow separation.

Unswept symmetrical circular-arc and double-wedge wing sections are studied at Mach numbers of 1·86 and 2·48. The aerofoil characteristics are derived from pressures measured on the wing surfaces and are compared with the theoretical values.

With the aid of schlieren photography the separation from the aerofoils is examined. The results obtained from experiments in which breakaway from a flat plate was induced by a forward-facing step[1] and a backward-facing step[2] on the plate are applied in an appendix, in assessing the pressures in the deadwater regions formed by the flow separation. The scope of the analysis by this method is limited by the inadequacy of the results obtained from the step experiments but a similarity between the flow in the two cases is illustrated.

* R.A.E. Rept. Aero. 2384, received 12th February, 1951.

2. *Equipment.*—The tests were made in a half-open jet supersonic wind tunnel (jet bounded on two sides only (*see* Fig. 2)), with a $5\frac{1}{2}$ in. $\times$ $5\frac{1}{2}$ in. working-section, using dry air. Nozzles giving Mach numbers 1·86 and 2·48 were used, the corresponding Reynolds numbers being $0{\cdot}66 \times 10^6$ and $0{\cdot}5 \times 10^6$ based on the wing chord. The wings were mounted on the test rig shown in Fig. 1. The two aerofoils tested were of symmetrical bi-convex (circular-arc) and double-wedge sections. They completely spanned the tunnel and had a chord of 2 in. and a thickness to chord ratio of 10 per cent. The holes for recording pressures were on the top surface only, spaced every 0·1 in. chordwise, except near the leading and trailing edges where the thin section made it impracticable; the distances of the nearest pressure hole from the leading and trailing edges was 0·2 in. for the bi-convex wing and 0·3 in. for the double-wedge wing. The line of holes was staggered relative to the stream direction to minimise the effect of disturbance from holes upstream on those downstream and the position was such as to be outside the influence of disturbances from the wing tips or supports.

The size of the aerofoils was such that all disturbances reflected from the tunnel walls were well behind the aerofoils over the range of incidence studied, and the measured pressures therefore apply to unswept two-dimensional wings. The incidence range was limited by tunnel blockage to $\pm$ 14 deg at $M = 1{\cdot}86$ and $\pm$ 16 deg at $M = 2{\cdot}48$. Fig. 2 shows the test rig in position in the wind tunnel.

A single hole in the lower surface of each aerofoil was used with the corresponding one in the upper surface for determining the position of zero incidence, the aerofoil being used virtually as a yawmeter.

3. *Test Procedure and Results.*—3.1. *Wing Surface Pressure Distributions.*—The pressure at each hole in both aerofoils was measured over the range of incidence from — 16 deg to + 16 deg at $M = 2{\cdot}48$ and — 14 deg to + 14 deg at $M = 1{\cdot}86$. In Figs. 3 to 6 these pressures, made dimensionless by dividing by the tunnel stagnation pressure, are plotted for every 2 deg incidence to give the chordwise pressure distributions. The curves obtained from the shock-expansion theory are inserted for comparison over the range where the theory is applicable and in general there is good agreement.

In general the curves show a tendency towards a higher pressure than the theoretical at the leading edge. The presence of the boundary layer at the mid-chord point of the double-wedge aerofoil causes the expansion to start ahead of the mid-chord point, and finish after it. The expansion influences the surface pressures roughly 10 per cent of the chord in each direction which is of the order of 7 boundary-layer thicknesses in each direction.

Flow separation occurs towards the trailing edge of the aerofoils at all positive incidences and at $M = 2{\cdot}48$ is apparent on the circular-arc aerofoil at — 2 deg incidence (Fig. 6) as shown by the increase in pressure. The breakaway takes place with a weak shock which moves forward as the incidence is increased. Introducing oil through the rearmost hole on the double-wedge aerofoil showed the reverse flow in the dead-water region associated with separation. The point to which the oil moved forward is shown in Fig. 4. The point of separation as denoted by this method depends on the surface tension of the oil used and appears to agree with the point of separation as denoted by the pressure measurements and schlieren photographs (Fig. 7) only when the angle the separated flow makes with the surface is fairly large. At the negative incidences the pressures near the trailing edge show, especially at the lower Mach number, $M = 1{\cdot}86$, a tendency to a lower pressure than the theoretical due, presumably, to the lower pressure in the dead-water region being transmitted upstream through the boundary layer.

The linear theory for predicting the aerofoil pressures can be used over a very limited range of incidence before the theory breaks down and in the range where the theory can be applied there is poor agreement with experiment.

The general shape of the pressure curves is not altered noticeably when the leading edge shock-wave is detached as is the case for the circular-arc aerofoil at $M = 1{\cdot}86$ above $\pm$ 9 deg incidence (Fig. 5). From schlieren photographs an over-expansion can be seen round the leading edge at incidences above 10 deg but the pressure holes are not close enough to the leading edge to record it.

3.2. *Boundary-layer Traverse on Double-wedge Aerofoil.*—A traverse was made with a total-head tube (0·02 in. outside diameter) through the boundary layer on the double-wedge aerofoil 0·7 in. from the leading edge at 6 deg incidence and $M = 2{\cdot}48$ (Fig. 8). The profile is characteristic of a laminar layer.

When studying the flow separation near the trailing edge of the aerofoils (section 3.4), wires are used to disturb the boundary layer. Fig. 8 includes a traverse through the boundary layer on the double-wedge aerofoil with wires, for the same conditions as the traverse of the undisturbed layer. There is an increase in thickness and the profile now is characteristic of a turbulent layer. There is a noticeable loss of total-head pressure in the main stream due to the shocks caused by the wires which suggests a drawback in the use of wires for producing turbulent boundary layers.

3.3. *Aerofoil Characteristics.*—Except for the centre of pressure position the theoretical and experimental values of the aerofoil characteristics, over the range of incidence considered, are in good agreement.

The theoretical and experimental lift coefficients for both aerofoils are plotted in Figs. 9 and 10. The disagreement between experiment and theory is never more than 5 per cent except for the double-wedge aerofoil at high incidences at $M = 1{\cdot}86$ when the discrepancy is about 10 per cent. Otherwise the curves are practically independent of aerofoil shape and vary only with Mach number. Even after the shock-wave at the leading edge detaches, the linear theory gives a good approximation to the experimental values. The loss of lift due to separation is a very small percentage of the total lift.

The drag coefficients are plotted in Figs. 11 and 12. The coefficients for the double-wedge aerofoil are less than for the circular-arc. The spreading of the expansion at the mid-chord results in a saving of roughly 5 per cent over the theoretical. The lift/drag ratios (Figs. 13 and 14) for the double-wedge are greater than for the circular-arc, the maximum lift/drag ratio being 5·1 as against 4·35 at $M = 1{\cdot}86$, and 5·0 as against 4·3 at $M = 2{\cdot}48$. There is, thus, little change with Mach number but a noticeable difference due to the aerofoil shape. The maxmum lift/drag ratio occurs at roughly 6 deg in all cases.

In Figs. 15 and 16 the position of the centre of pressure relative to the leading edge is plotted against incidence. There is a noticeable disagreement between theory and experiment. The experimental values lie much closer to the values obtained from the shock-expansion theory than to the values obtained from the linear theory. The effect of the separation on the centre of pressure position is shown at 8 deg incidence. For the double-wedge aerofoil separation accounts for about half the difference between the shock-expansion theory and experiment, the effect of the expansion spreading at the mid-chord point being negligible (Fig. 15); for the circular-arc aerofoil the separation accounts for nearly all the difference between the shock-expansion theory and experiment. The difference between the linear theory and the shock-expansion theory indicates the effect of neglecting second-order terms.

3.4. *Schlieren Observation.*—Schlieren observation was used to study the effect on the flow over the aerofoils of disturbing the boundary layer. Comparison was made between the undisturbed boundary layer, and the boundary layer disturbed by wires glued on the upper surface of the aerofoils near the leading edge. At $M = 2{\cdot}48$ differences were slight.

At $M = 1{\cdot}86$ the onset of breakaway was always delayed by the presence of wires on either aerofoil. When the breakaway did occur there were noticeable differences between the two cases. Fig. 17 shows the double-wedge aerofoil at 6 deg incidence ($M = 1{\cdot}86$). The undisturbed (laminar) boundary layer gradually separates just aft of the mid-chord with the formation of a compression fan; the disturbed (turbulent) boundary layer is still completely attached to the aerofoil up to the trailing edge. At 14 deg incidence (Fig. 18) the flow has separated with both boundary layers but the breakaway is different in each case. The laminar layer separates just

aft of the mid-chord whereas the turbulent layer separates only a very small distance forward of the trailing edge. At 14 deg incidence (Fig. 19) the circular arc aerofoil shows similar types of breakaway, the laminar boundary layer separating much further upstream than the turbulent layer.

It should be noted when comparing the separation of the flow for the two cases with and without wires, that besides producing turbulence in the boundary layer the presence of wires also appreciably increased the thickness of the boundary layer.

4. *Conclusions.*—Some of the phenomena, which result from the viscous nature of the airflow over aerofoils, and their effect on the practically important aerofoil characteristics have been studied. The flow separation from the aerofoils has been examined by means of schlieren and a brief analysis (Appendix) made to identify the separation with that from right-angled steps[1,2].

The surface pressure distributions over the aerofoils did not deviate much from the shock-expansion theory except in the region where the flow separated. The aerofoil characteristics, C_L, C_D and L/D, derived from the pressure distributions were also in good agreement with both theories and the discrepancy was usually not more than 5 per cent. The difference between the experimentally and theoretically derived centre of pressure position, however, was affected more by the separation and the inaccuracy of the pressure distribution as predicted by the linear theory; the centre of pressure position was between 35 per cent and 40 per cent of the chord from the leading edge in all cases, and separation accounted for a move of about 4 per cent of the chord at 8 deg incidence.

Schlieren observation showed the different types of separation associated with laminar and turbulent boundary layers. Making the boundary layer turbulent by means of wires was found to delay separation.

The pressure rise at the point of separation from the aerofoils was found not to be a function of the size of the dead-water region after separation as was the case with the separation in front of a right-angled step on a flat plate; in some cases the pressure rise was increased with an increase in the size of the dead-water region and in other cases decreased. The pressure ratio across the shock where the flow from both sides of the dead-water region comes together (at B, Fig. 22) was found to increase, in all cases, as the size of the dead-water region increased. This was in accordance with what was found from the flow over backward facing right-angled steps. Here, increasing the step height, and consequently the size of the dead-water region, increased the pressure ratio across the shock at the point of reattachment of the flow behind the dead-water region.

REFERENCES

No.	*Author*	*Title, etc.*
1	D. Beastall and H. Eggink ..	Some Experiments on Breakaway in Supersonic Flow. R.A.E. Tech. Note Aero. 2041.
2	D. Beastall and H. Eggink ..	Some Experiments on Breakaway in Supersonic Flow (Part II). R.A.E. Tech. Note Aero. 2061.

APPENDIX I

1. *Analysis of the Flow Separation From the Aerofoils.*—In Refs. 1 and 2 experiments are described which deal with the two-dimensional flow over forward-facing (Fig. 20) and backward-facing (Fig. 21) steps mounted on flat plates. The purpose of this analysis is to find the extent to which the results from these experiments can be applied to the flow separation from the aerofoils. Since the experiments were only a preliminary investigation of the flow over steps and were therefore incomplete, it was not expected that agreement with the aerofoil tests would be very close but it was intended that the analysis would serve to indicate whether agreement could be expected from more comprehensive tests.

1.1. *The Pressure Rise at the Point of Separation.*—In Ref. 1 a forward-facing step on a flat plate (Fig. 20) was used for inducing breakaway from the plate, with the formation of a dead-water region in the corner of the step. In a similar way the separation from the surface of an aerofoil takes place with a shock and the formation of a dead-water region (Fig. 22). In the experiments with the flow over a forward-facing step the ratio of the dead-water region pressure to the free-stream static pressure before separation, increased as the step height was increased for a given Mach number before separation, and was different if the boundary layer on the plate was laminar or turbulent; the pressure ratio also increased as the Mach number before separation increased. If the mechanism for producing the dead-water region pressures in the two cases is the same we should expect the pressure ratio across the shock at breakaway from the aerofoils to increase with increase in 'step height' and Mach number ahead of the shock. The step height of the dead-water region behind the aerofoil is defined (Fig. 22) as the height, h, the perpendicular distance from B on to the tangent at A. In Tables 1 and 2 are the results obtained from the aerofoil tests. The pressure ratios across the shock at separation were taken from Figs. 3 to 6 and the Mach numbers were derived from these pressures; the step heights were measured from the schlieren photographs.

That the pressure rise at the point of separation from the aerofoils is not a function of the step height as defined here, can be seen from the fact that for the double-wedge aerofoil at $M = 2{\cdot}48$ the pressure ratio across the shock decreases as the step height increases whereas for the circular-arc aerofoil the ratio increases. The shock strength at the point of separation must, therefore, be governed by some other requirement of the flow.

1.2. *The Dead-water Region Pressure.*—In Ref. 2 a backward-facing step on a flat plate (Fig. 21) was used for inducing breakaway of the flow with the formation of a dead-water region in the corner of the step. In this case the dead-water region pressure decreased as the step height was increased, for a given Mach number before the step. The relationship between the pressure ratio, P_2/P_1, across the shock at the point of reattachment to the plate and the height of the step was obtained for laminar and turbulent boundary layers for a Mach number $= 2{\cdot}48$ on the step.

There is a similarity between the flow over a backward-facing step and the flow separation from an aerofoil. In both cases the main-stream flow is in contact with a dead-water region, after which it is returned through a shock to nearly the free-stream direction. The main difference is that the dead-water region behind the aerofoil is bounded by the flow from both sides of the aerofoil whereas the dead-water region behind the step is only bounded on one side by the airflow.

The pressure rise across the shock at the point of reattachment to the plate given by the step experiments for given step heights is now applied to the aerofoil tests to predict the pressure rise across the shock through which the flow is returned to the free-stream direction. The following procedure was adopted.

Curve A, Fig. 23, is taken from the experiments with a backward-facing step and gives the pressure ratio, P_2/P_1, across the shock at the point of reattachment of the flow to the back plate for a laminar boundary layer on the step and a free-stream Mach number of $2{\cdot}48$. Thus

$P_1/P_2 \simeq 0{\cdot}06$ corresponding to $M_2 = 2{\cdot}48$. The step heights as defined (Fig. 22) by AF (for the flow over the upper surface of the aerofoil) and GD (for the flow over the lower surface) were measured from the schlieren for a range of incidences of the circular-arc aerofoil when the free-stream Mach number was $2{\cdot}48$. At each incidence the pressure ratios P_2/P_1 given by curve A for steps of height AF and GD were used to obtain the values of P_1/P_0 the dead-water region pressures (since $P_2/P_0 \simeq 0{\cdot}06$). The mean of the two values of P_1/P_0 was used to obtain a value of P_2/P_1 which is shown in curve B Fig. 23. The measured P_2/P_1 (from the aerofoil tests) is plotted for comparison (curve C, Fig. 23) and Table 3 gives the complete results.

The above is repeated for the double-wedge aerofoil at $M = 2{\cdot}48$ (Fig. 24 and Table 4). Agreement between the derived and measured pressure ratios is quite good in both cases.

1.3. *Discussion of Analysis.*—It is apparent from this brief analysis that the data provided by the experiments in the flow over forward-facing and backward-facing steps is insufficient to predict fully the flow configuration over an aerofoil when separation occurs. The point of separation is indeterminate and the flow over a forward-facing step appears to have no bearing on the pressure rise at the point of separation. However, when allowance is made for the different boundary layers on the aerofoils and the steps there seems to be a similarity between the flow over a backward-facing step and the separated flow from aerofoils. The mechanism by which the dead-water region pressures are governed is still obscure although the pressures are known to vary with step height and boundary layers.

The flow over steps does not appear to have sufficient resemblence to the separation of flow from aerofoils to make a more comprehensive study worthwhile at present.

TABLE 1

Double-Wedge Aerofoil

Pressure Rise across the Shock at Separation

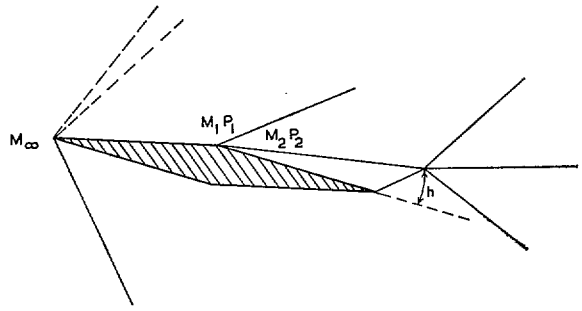

$M_\infty = 1{\cdot}86$

Incidence (deg)	$\frac{P_1}{P_0}$	$\frac{P_2}{P_0}$	$\frac{P_2}{P_1}$	h	M_1
8	0·076	0·090	1·185	0·03	2·33
10	0·067	0·081	1·209	0·04	2·41
12	0·060	0·074	1·233	0·05	2·48
14	0·058	0·068	1·172	0·06	2·51

$M_\infty = 2{\cdot}48$

Incidence (deg)	$\frac{P_1}{P_0}$	$\frac{P_2}{P_0}$	$\frac{P_2}{P_1}$	h	M_1
4	0·031	0·041	1·323	0·03	2·91
6	0·028	0·037	1·322	0·06	2·98
8	0·026	0·033	1·270	0·08	3·03
10	0·0255	0·030	1·176	0·11	3·04
12	0·025	0·027	1·080	0·14	3·06
14	0·024	0·025	1·041	0·17	3·08

TABLE 2

Circular Arc Aerofoil

Pressure Rise across the Shock at Separation

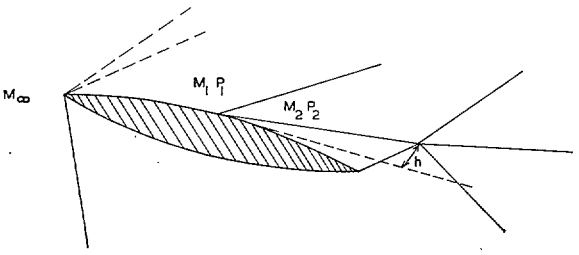

$M_\infty = 1{\cdot}86$

Incidence (deg)	$\frac{P_1}{P_0}$	$\frac{P_2}{P_0}$	$\frac{P_2}{P_1}$	h	M_1
2	0·106	0·115	1·084	0·03	2·12
4	0·100	0·109	1·090	0·03	2·16
6	0·093	0·103	1·108	0·03	2·20
8	0·086	0·096	1·117	0·06	2·25
10	0·077	0·088	1·129	0·06	2·32
12	0·073	0·082	1·122	0·06	2·36
14	0·064	0·075	1·171	0·08	2·44

$M_\infty = 2{\cdot}48$

Incidence (deg)	$\frac{P_1}{P_0}$	$\frac{P_2}{P_0}$	$\frac{P_2}{P_1}$	h	M_1
0	0·040	0·045	1·125	0·03	2·75
2	0·038	0·043	1·132	0·03	2·78
4	0·035	0·041	1·171	0·06	2·83
6	0·033	0·038	1·152	0·08	2·87
8	0·030	0·036	1·200	0·08	2·94
10	0·027	0·033	1·222	0·11	3·01
12	0·024	0·030	1·250	0·11	3·08
14	0·022	0·029	1·318	0·14	3·14
16	0·021	0·027	1·286	0·17	3·17

TABLE 3

Circular-arc Aerofoil at $M_\infty = 2{\cdot}48$: Comparison of P_2/P_1 across Shock behind Aerofoil predicted from Step Experiments with Measured Pressures

Incidence (deg)	AF (Fig. 22)	GD (Fig. 22)	Mean step ht. $H_2 = \frac{AF + GD}{2}$	For h = AF		For h = GD		Mean $\frac{P_1}{P_0}$	Mean $\frac{P_2}{P_1}$	Measured $\frac{P_2}{P_1}$
				$\frac{P_2}{P_1}$	$\frac{P_1}{P_0}$	$\frac{P_2}{P_1}$	$\frac{P_1}{P_0}$			
6	0·13	0·03	0·08	2·371	0·0253	1·271	0·0472	0·0363	1·65	1·54
8	0·16	0·04	0·10	2·575	0·0233	1·379	0·0435	0·0334	1·80	1·67
10	0·19	0·06	0·125	2·715	0·0221	1·600	0·0375	0·0298	2·01	1·82
12	0·24	0·04	0·140	2·927	0·0205	1·379	0·0435	0·0320	1·88	2·00
14	0·28	0·08	0·18	3·046	0·0197	1·869	0·0321	0·0259	2·32	2·07
16	0·31	0·10	0·205	3·125	0·0192	2·098	0·0286	0·0239	2·51	2·22

TABLE 4

Double-wedge Aerofoil at $M_\infty = 2{\cdot}48$: Comparison of P_2/P_1 across Shock behind Aerofoil predicted from Step Experiments with Measured Pressures

Incidence (deg)	AF (Fig. 22)	GD (Fig. 22)	Mean step ht. $H_2 = \frac{AF + GD}{2}$	For h = AF		For h = GD		Mean $\frac{P_1}{P_0}$	Mean $\frac{P_2}{P_1}$	Measured $\frac{P_2}{P_1}$
				$\frac{P_2}{P_1}$	$\frac{P_1}{P_0}$	$\frac{P_2}{P_1}$	$\frac{P_1}{P_0}$			
6	0·14	0·05	0·095	2·45	0·0245	1·56	0·0385	0·0315	1·906	1·62
8	0·16	0·06	0·110	2·60	0·0231	1·67	0·0360	0·0295	2·039	1·82
10	0·19	0·06	0·125	2·78	0·0216	1·67	0·0360	0·0288	2·082	2·00
12	0·22	0·07	0·145	2·90	0·0207	1·77	0·0339	0·0273	2·200	2·22
14	0·25	0·08	0·165	2·98	0·0202	1·88	0·0319	0·0260	2·304	2·40

(60241)

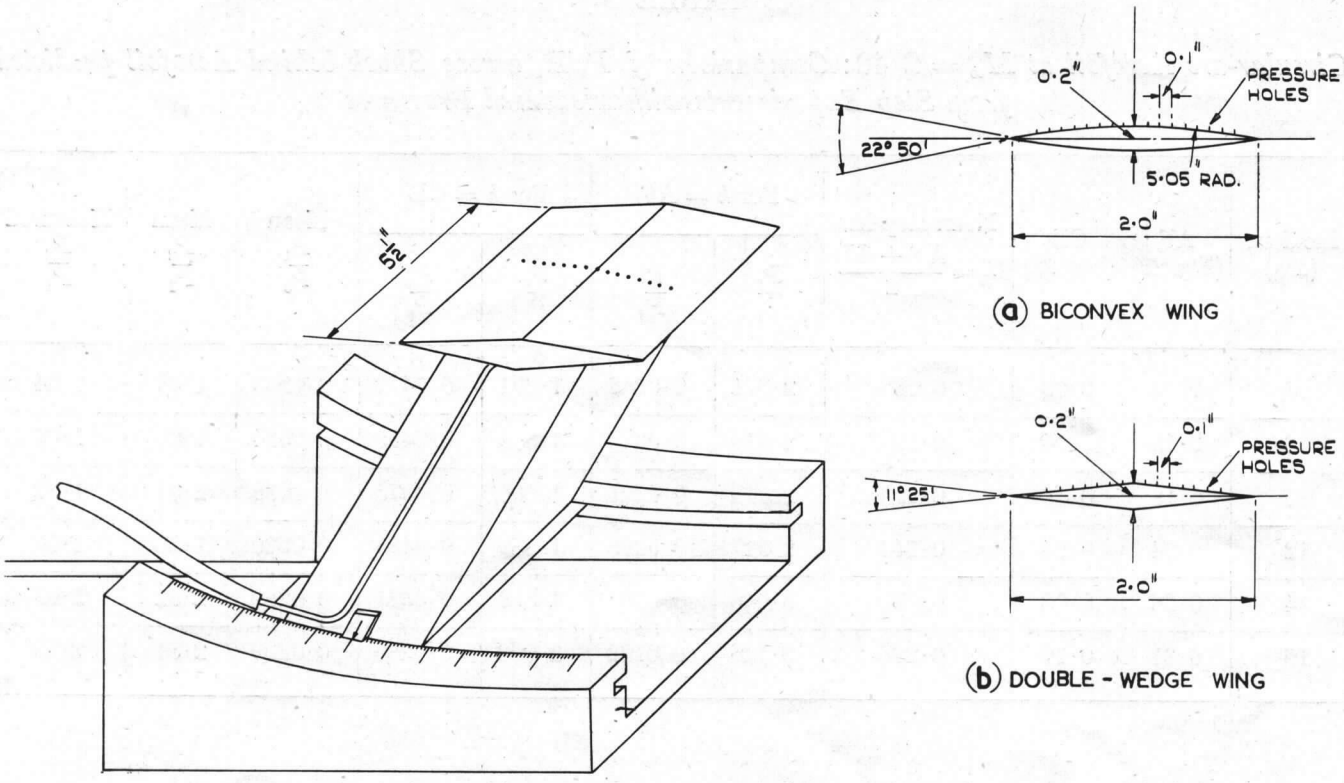

FIGS. 1, 1a and 1b. Aerofoil test rig.

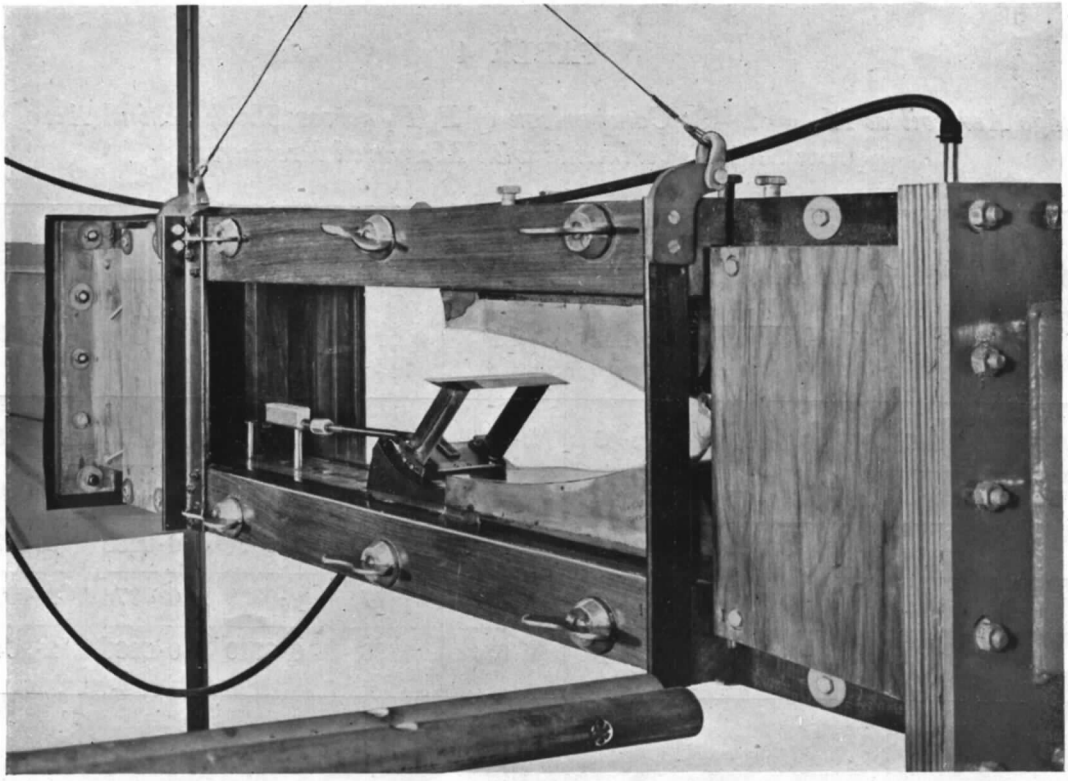

FIG. 2. Test arrangement in wind tunnel ($M = 2{\cdot}48$).

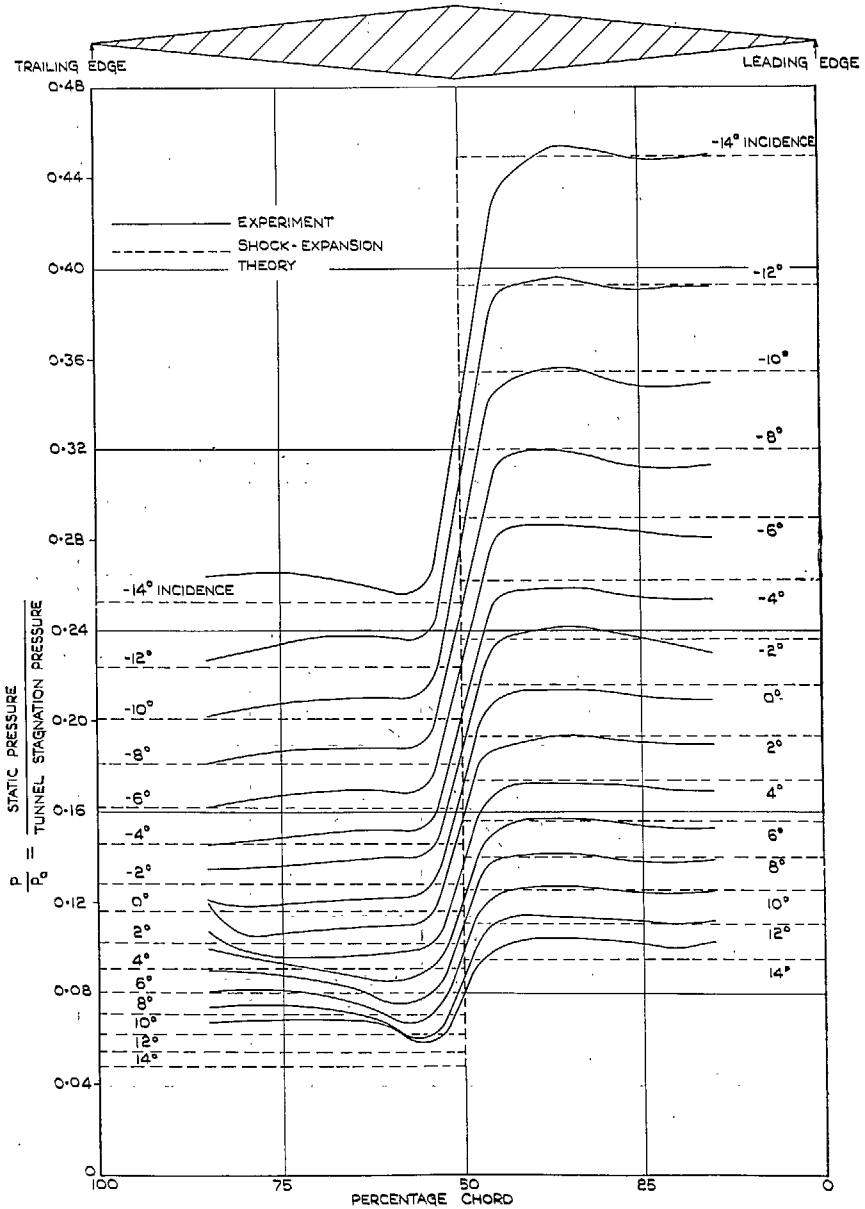

FIG. 3. Double-wedge wing: chordwise pressure distribution, on top surface at $M = 1{\cdot}86$.

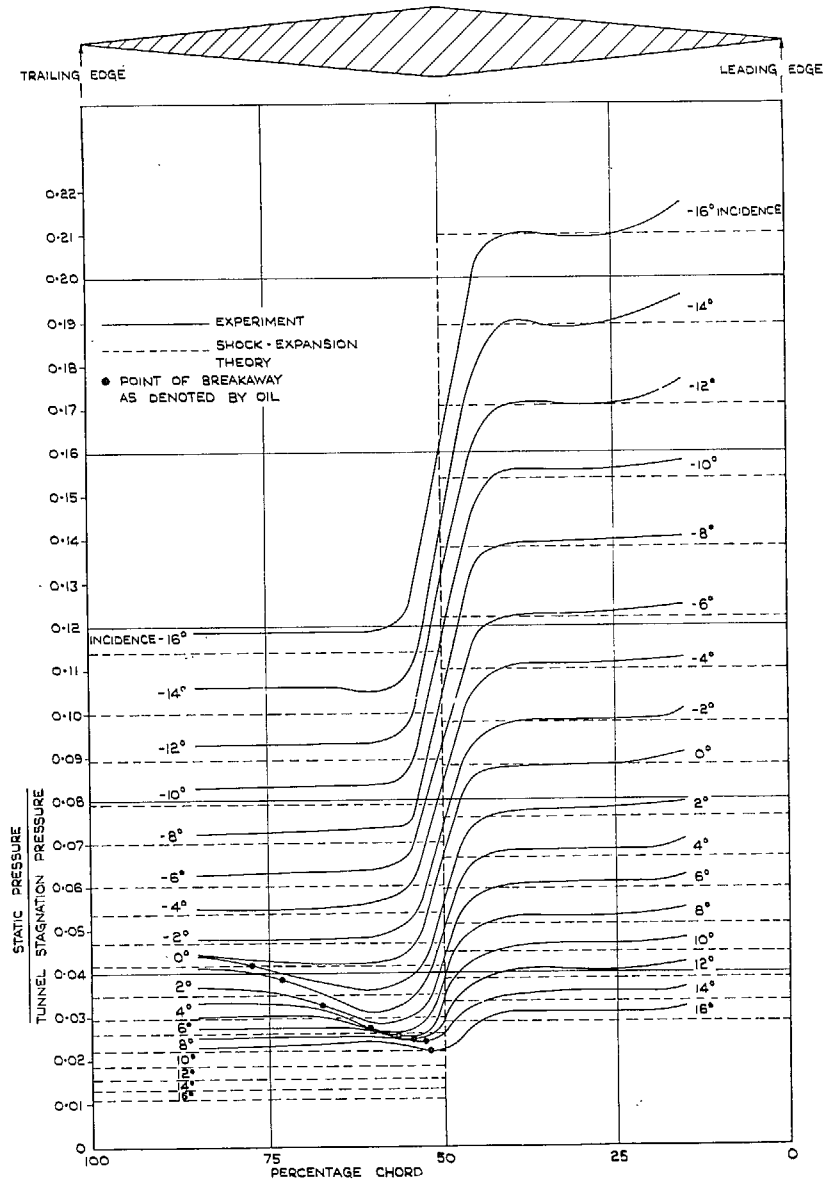

FIG. 4. Double-wedge wing: chordwise pressure distribution, on top surface at $M = 2{\cdot}48$.

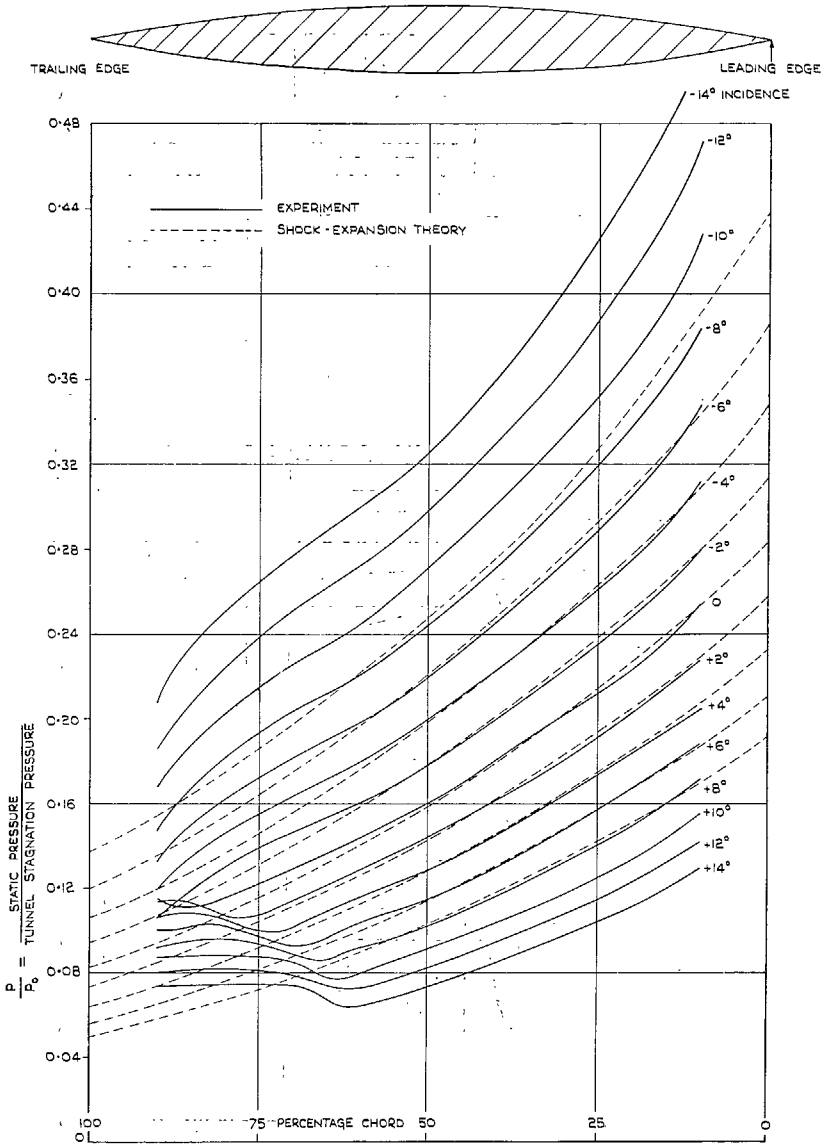

FIG. 5. Circular-arc wing : Chordwise pressure distribution, on top surface at $M = 1 \cdot 86$.

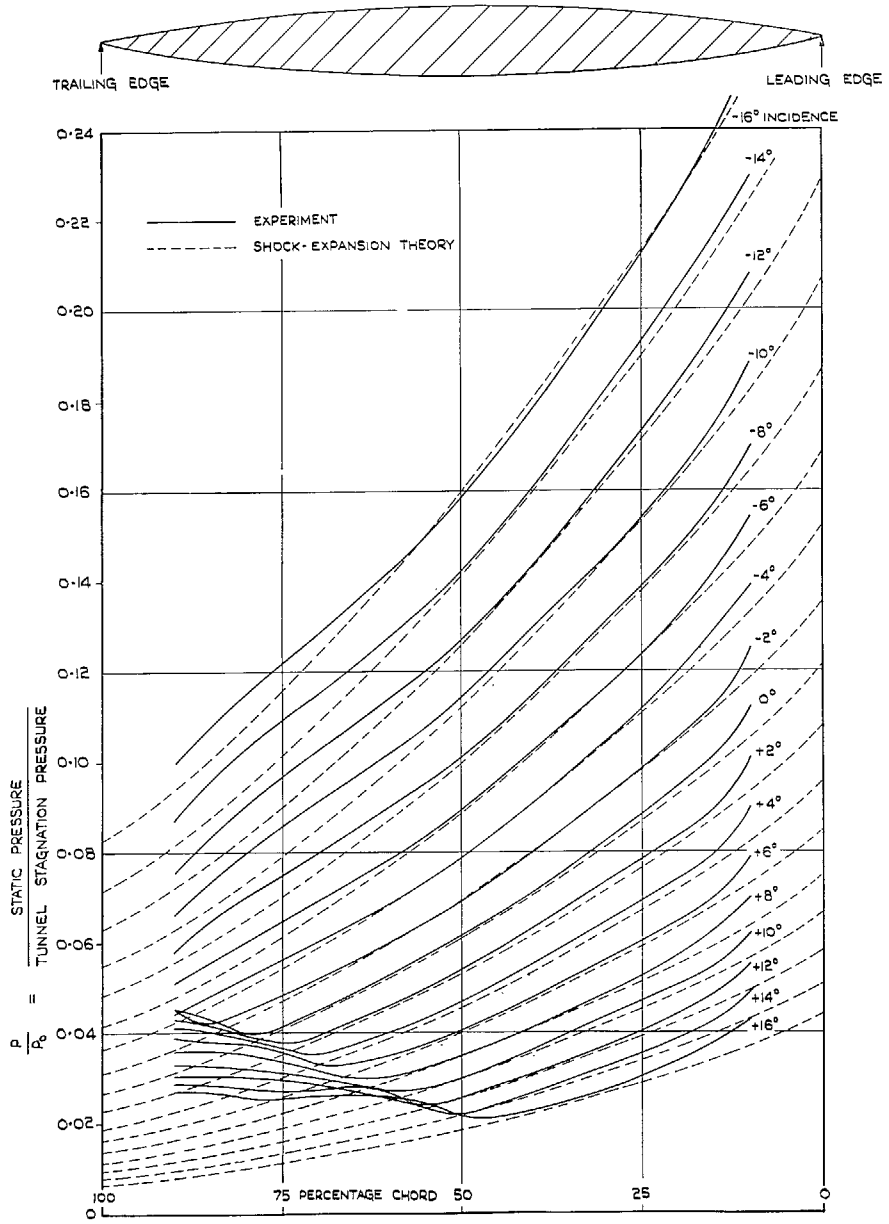

FIG. 6. Circular-arc wing : chordwise pressure distribution, on top surface at $M = 2 \cdot 48$.

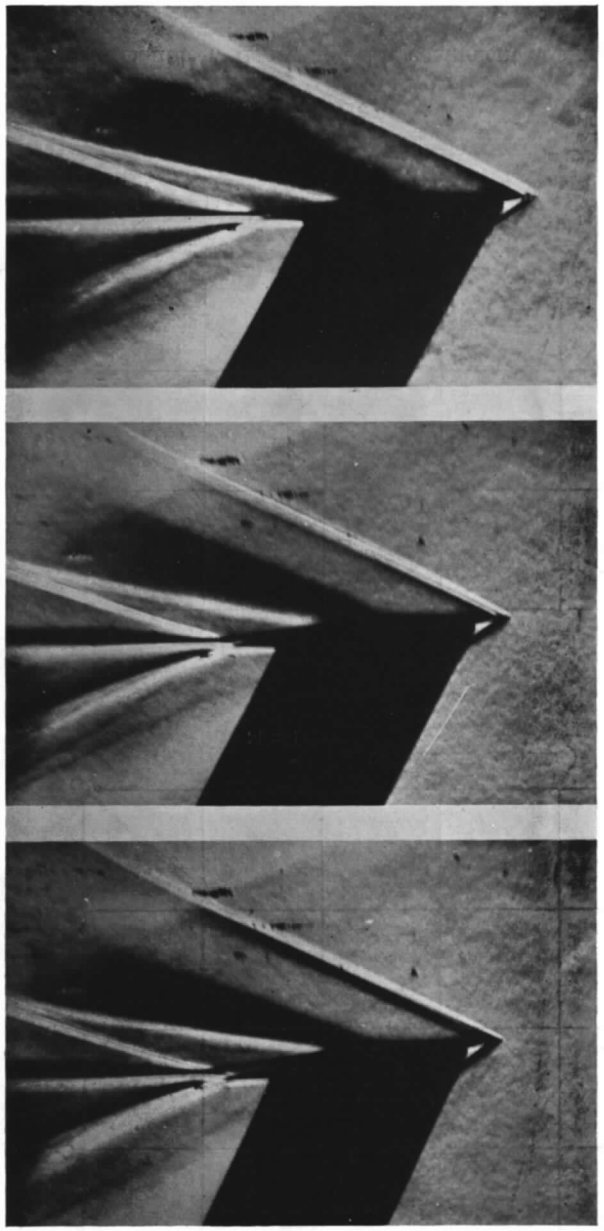

FIG. 7. Double-wedge aerofoil at $M = 2{\cdot}48$ showing forward movement of point of breakaway with increase in incidence.

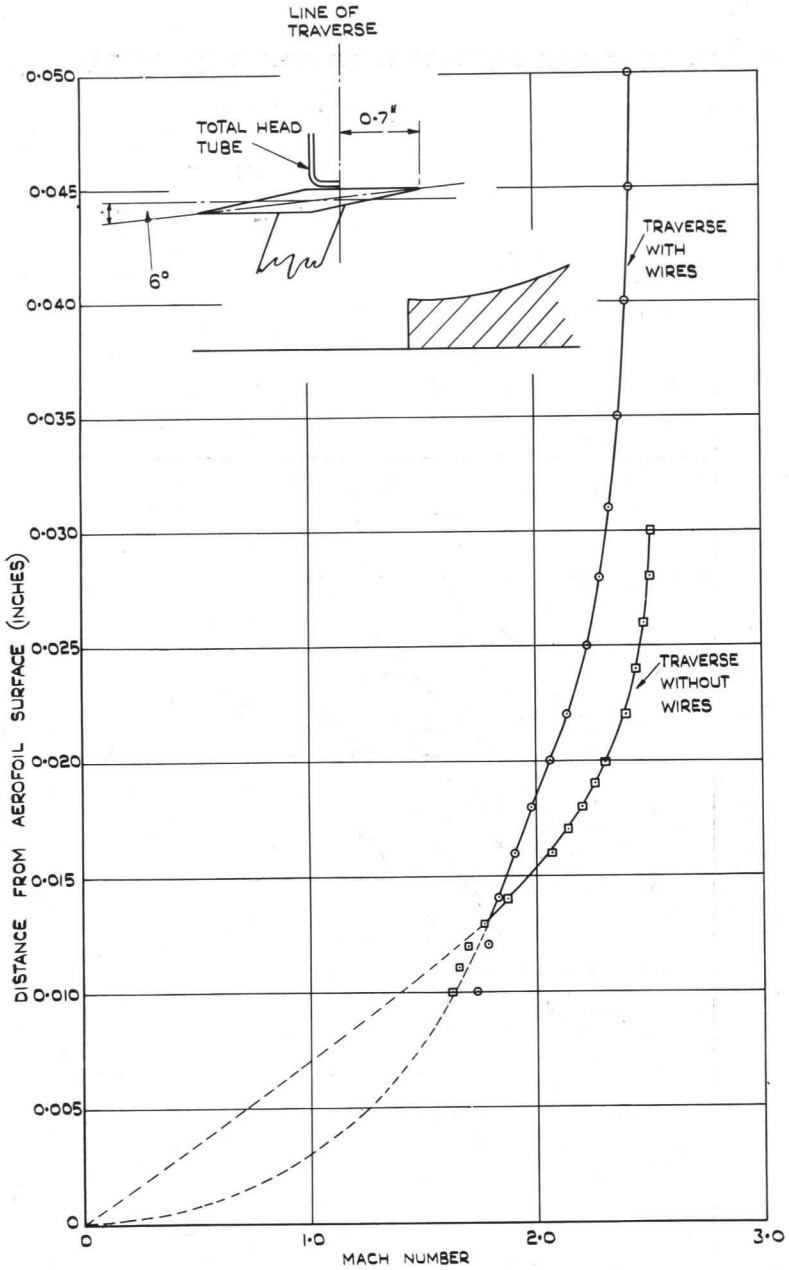

FIG. 8. Boundary-layer traverse of double-wedge wing at $M = 2{\cdot}48$ (line of traverse $0{\cdot}7$ in. from leading edge).

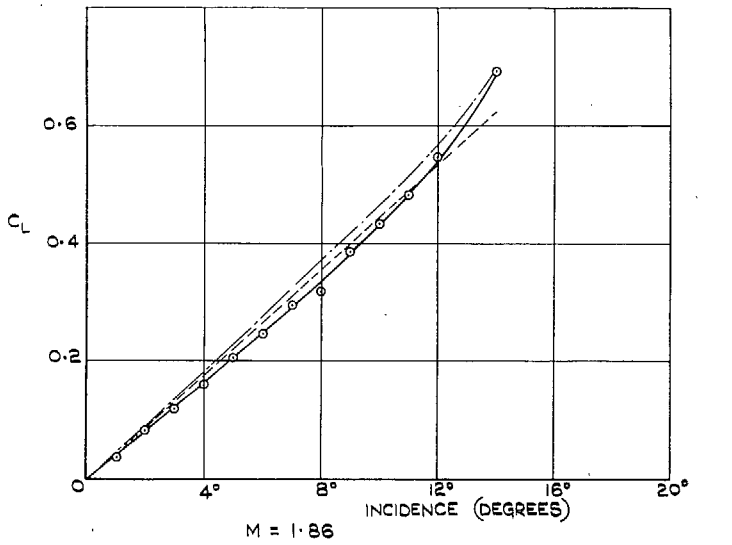

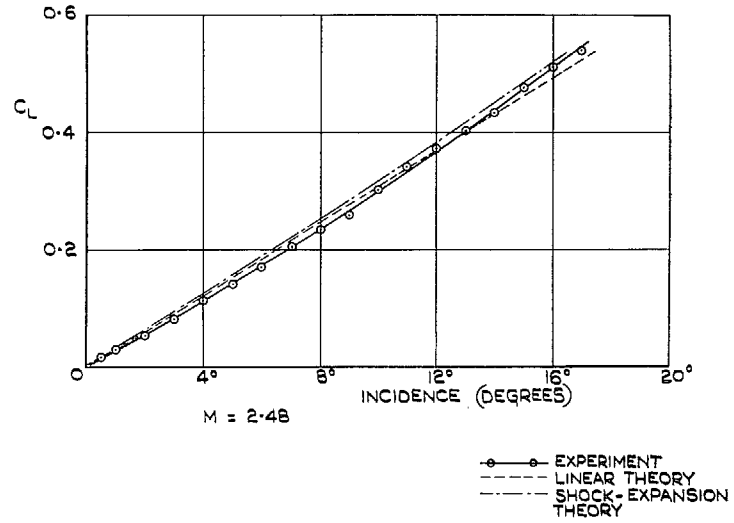

FIG. 9. Double-wedge wing : lift coefficient against incidence.

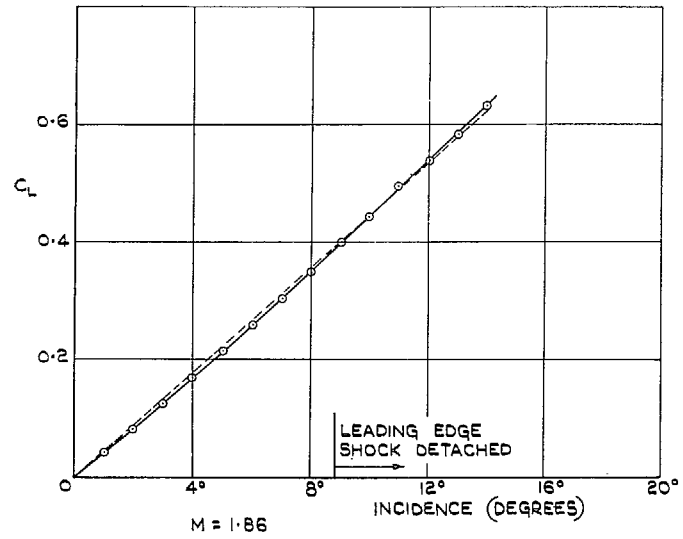

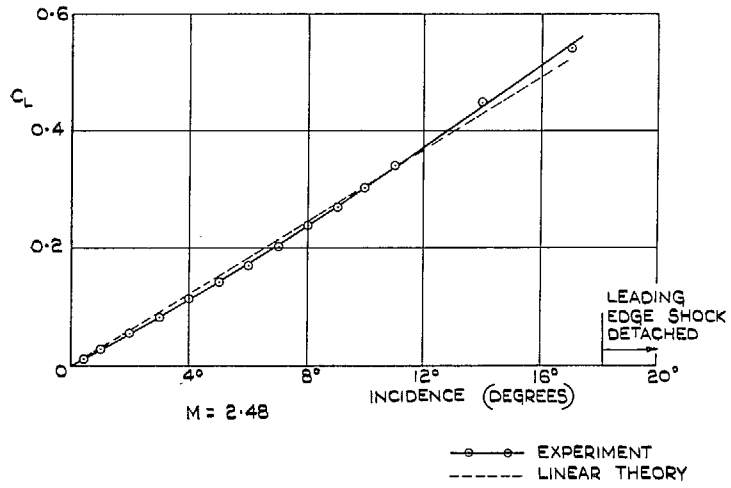

FIG. 10. Circular-arc wing : lift coefficient against incidence.

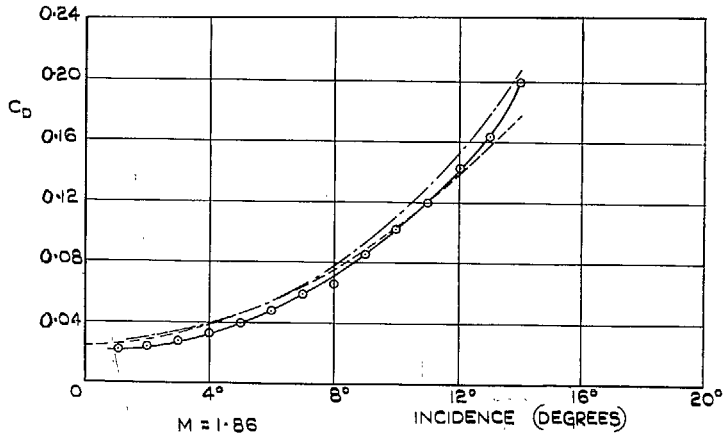

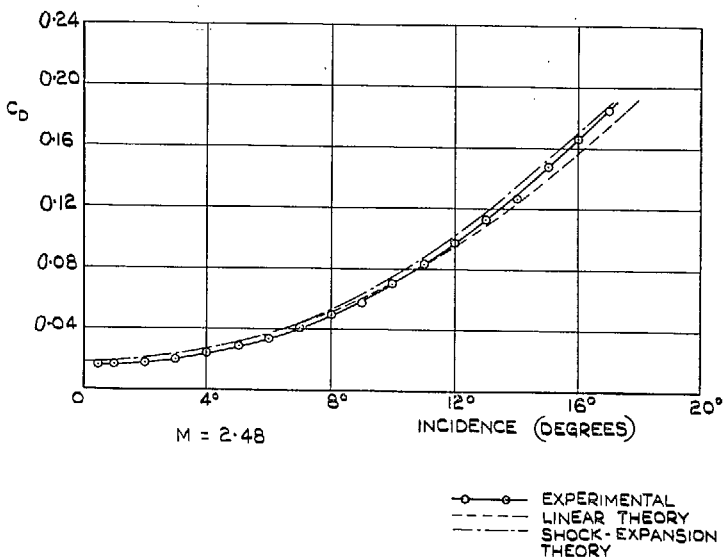

FIG. 11. Double-wedge wing : drag coefficient against incidence.

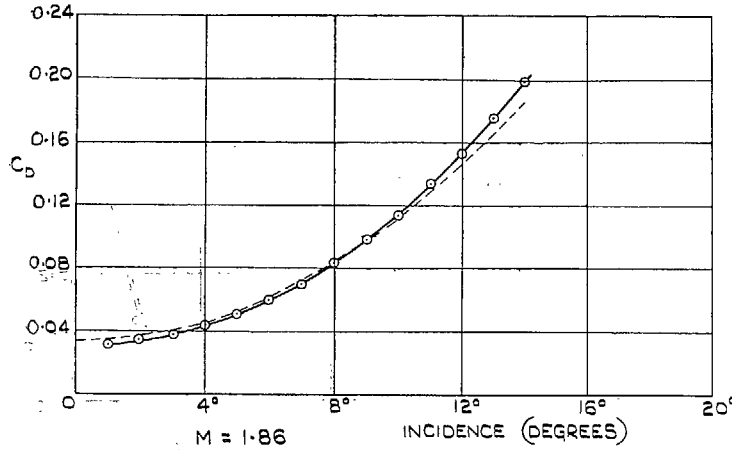

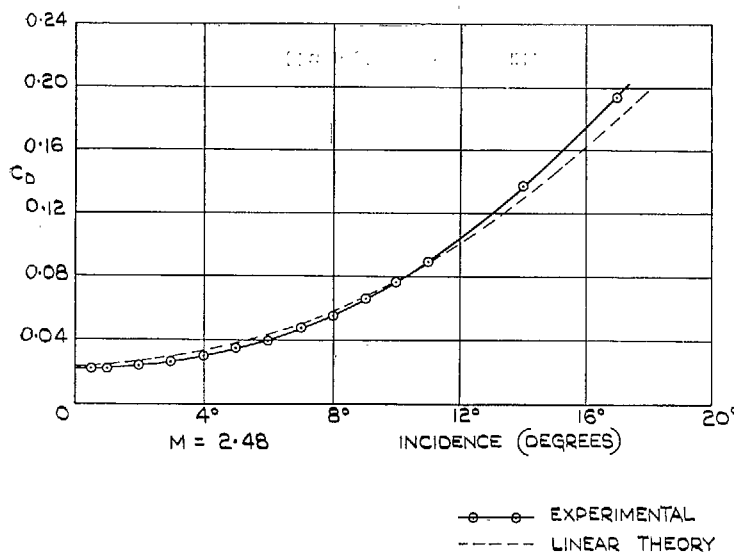

FIG. 12. Circular-arc wing : drag coefficient against incidence.

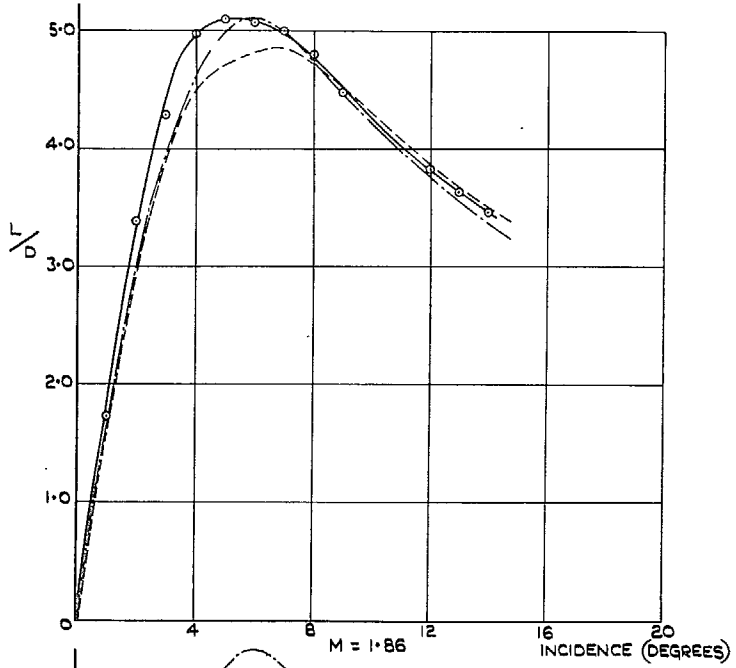

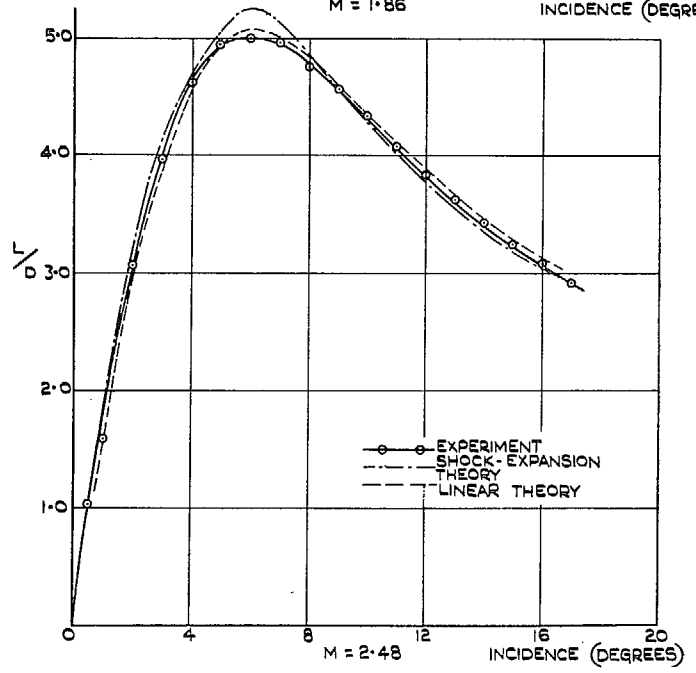

FIG. 13. Double-wedge aerofoil : lift/drag ratio against incidence.

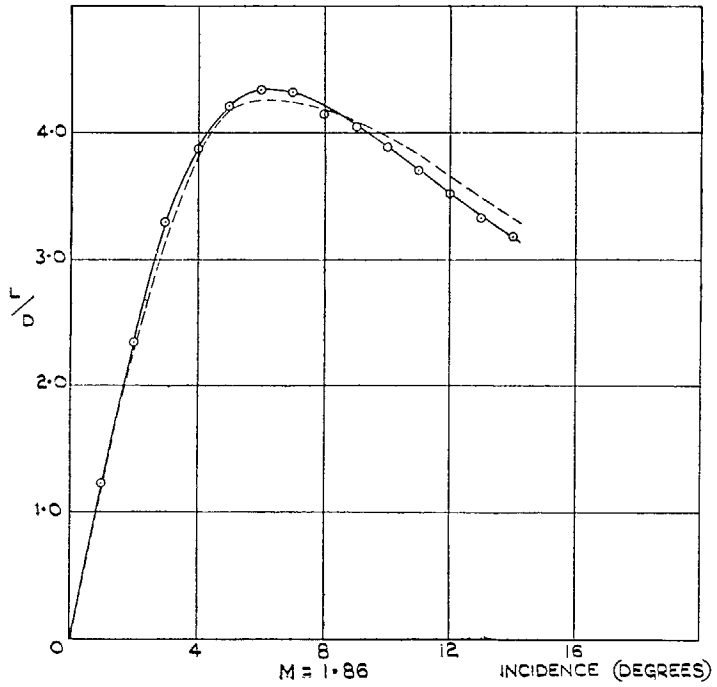

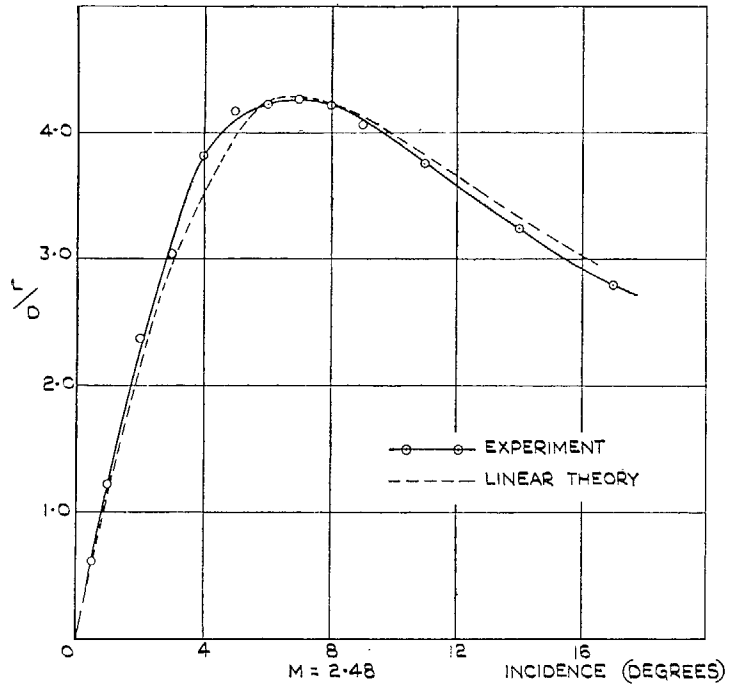

FIG. 14. Circular-arc aerofoil : lift/drag ratio against incidence.

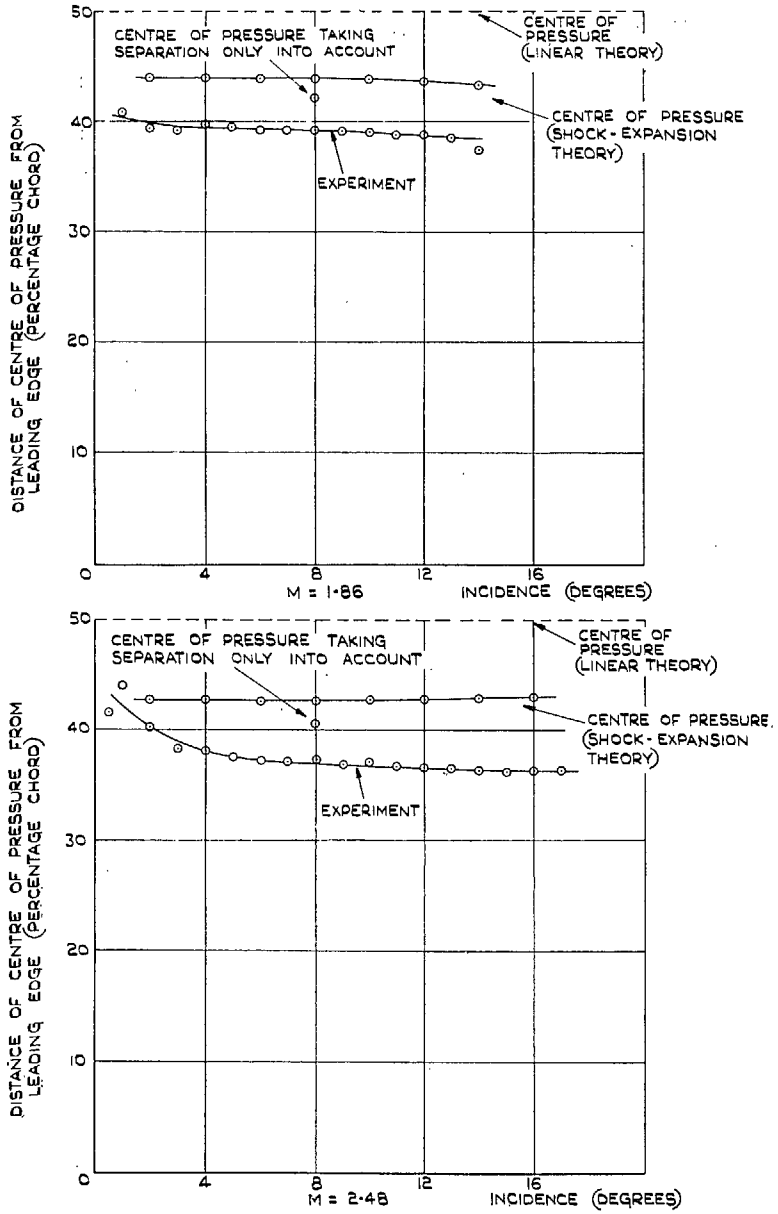

FIG. 15. Double-wedge aerofoil : distance of centre of pressure from leading edge against incidence.

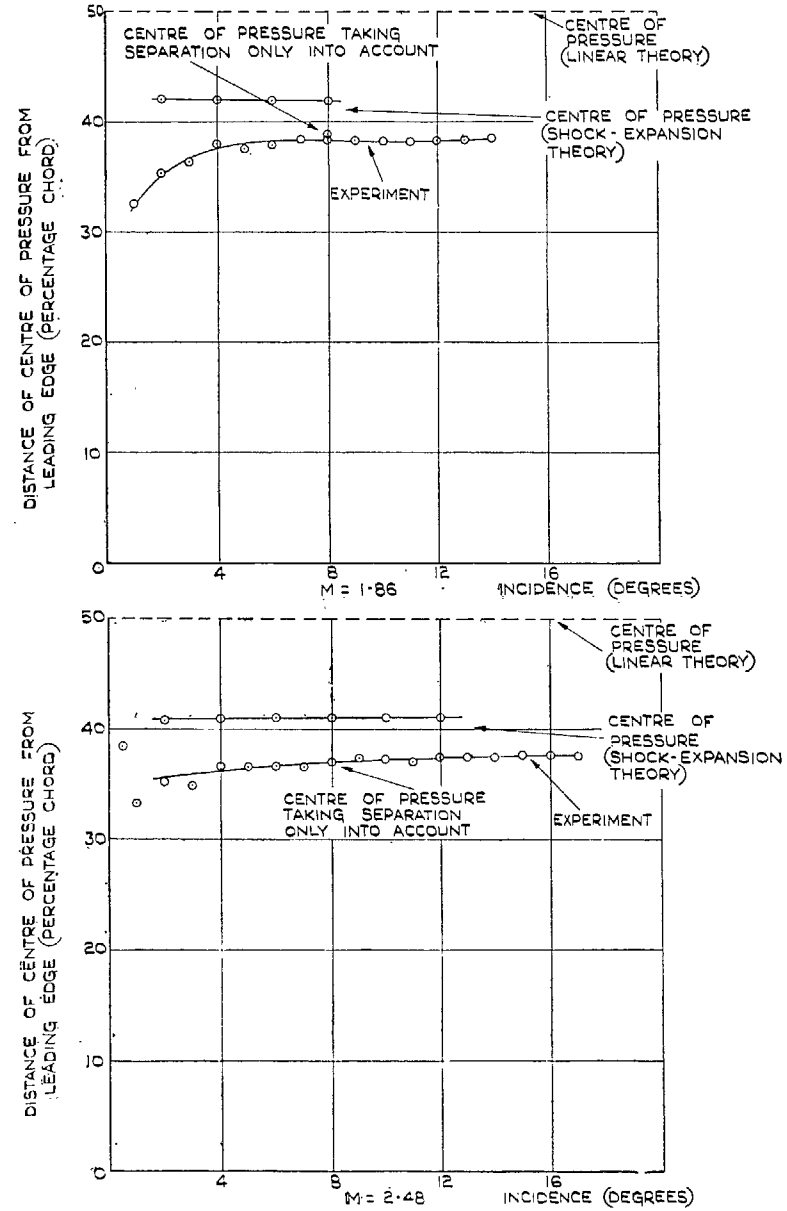

FIG. 16. Circular-arc aerofoil : distance of centre of pressure from leading edge against incidence.

a. Laminar boundary layer.

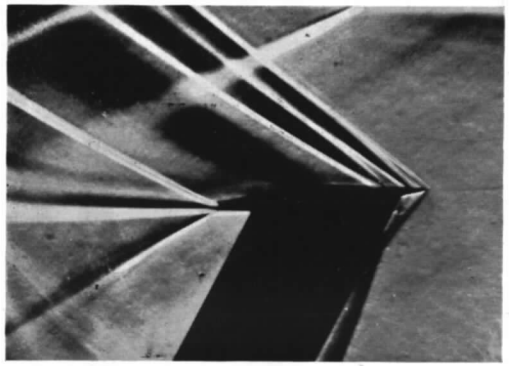

b. Turbulent boundary layer.

FIGS. 17a and 17b. Schlieren photographs of double-wedge aerofoil with laminar and turbulent boundary layers ($M = 1{\cdot}86$. Incidence 6 deg). Knife-edge horizontal.

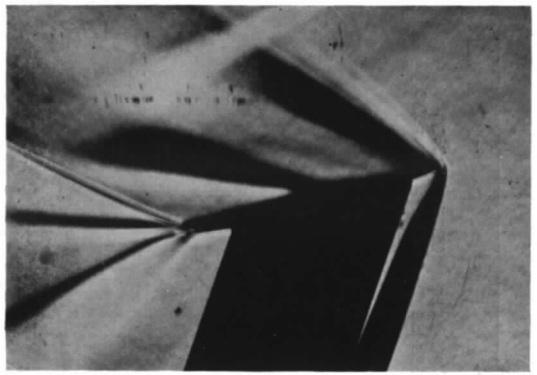

a. Laminar boundary layer.

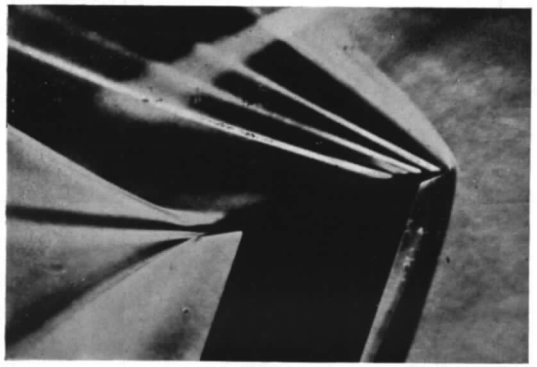

b. Turbulent boundary layer.

FIGS. 18a and 18b. Schlieren photographs of double-wedge aerofoil at 14 deg incidence ($M = 1{\cdot}86$).

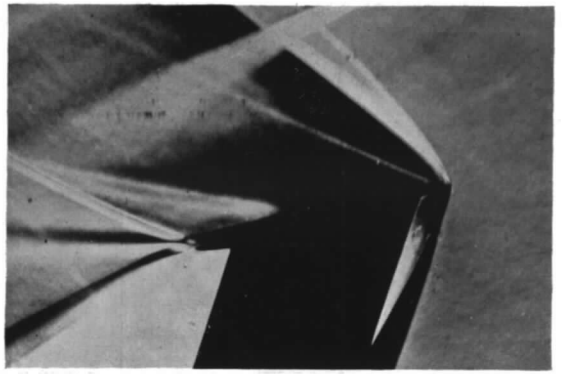

a. Laminar boundary layer.

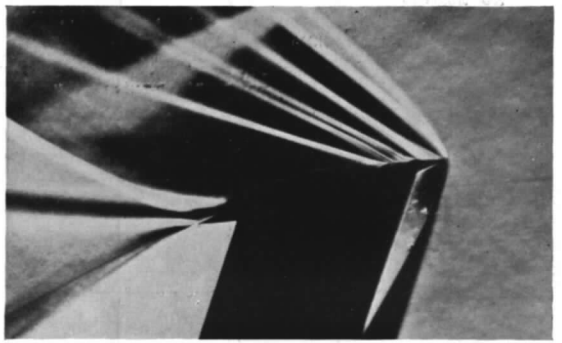

b. Turbulent boundary layer.

FIGS. 19a and 19b. Schlieren photographs of circular-arc aerofoil at 14 deg incidence ($M = 1{\cdot}86$).

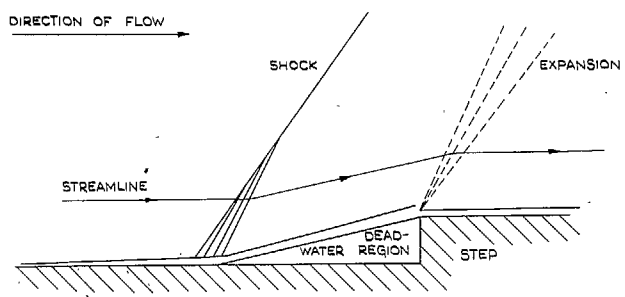

FIG. 20. Flow over a forward-facing step.

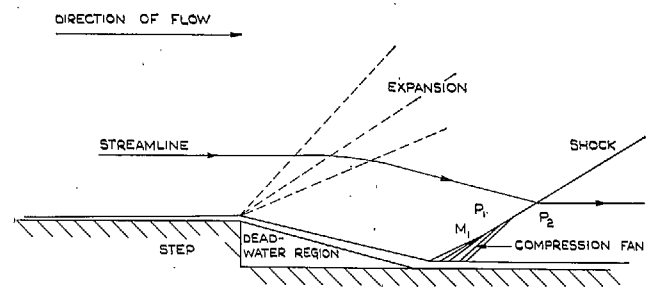

FIG. 21. Flow over a backward-facing step.

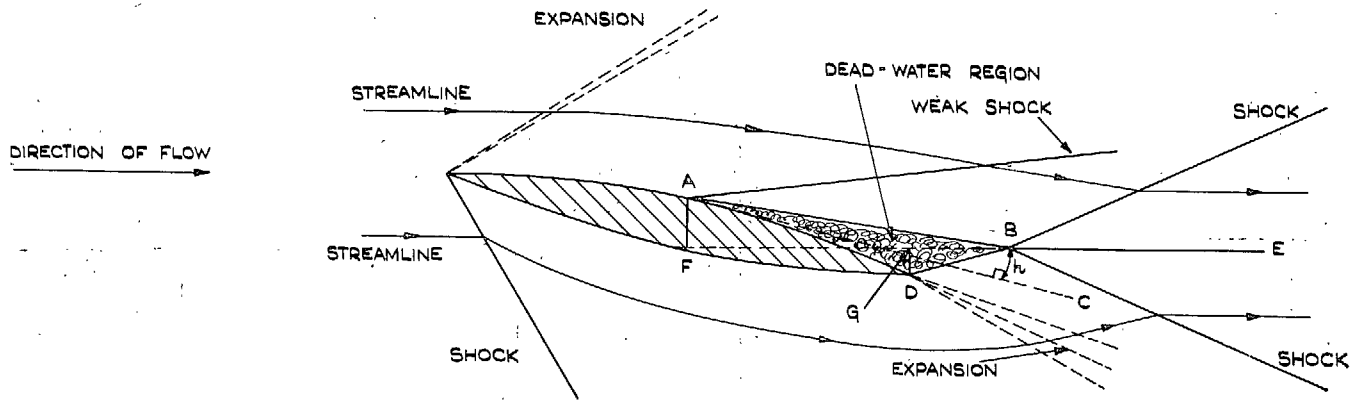

FIG. 22. Flow over two-dimensional aerofoil with separation.

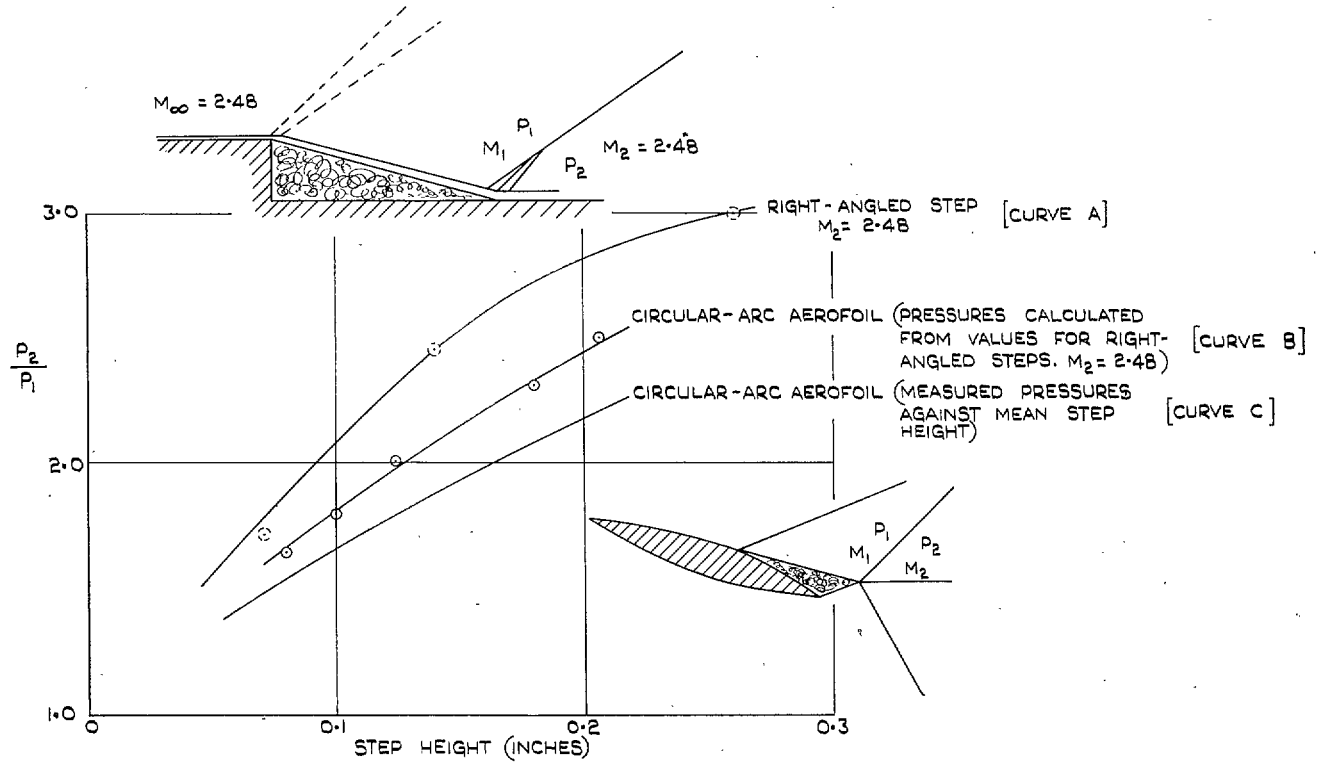

FIG. 23. Comparison of pressure ratio P_2/P_1 across shock behind circular-arc aerofoil and P_2/P_1 predicted from step experiments.

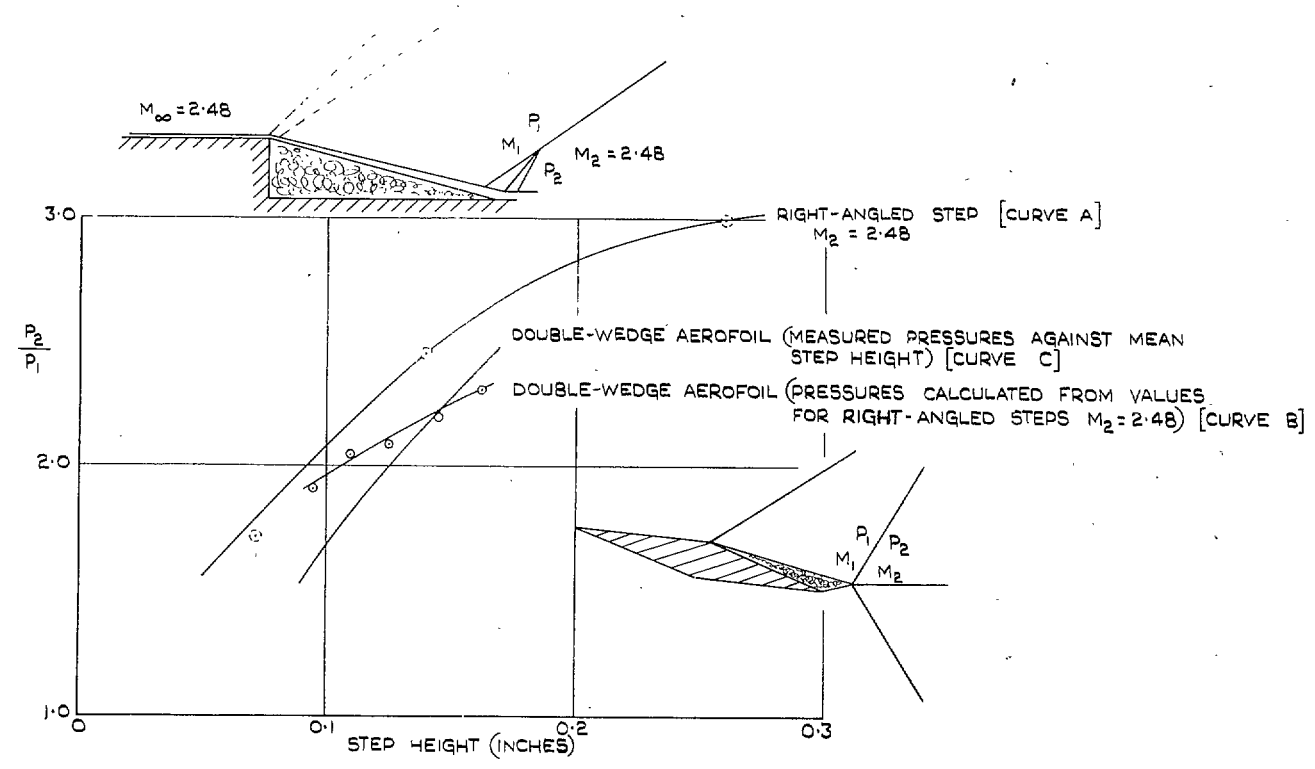

FIG. 24. Comparison of pressure ratio P_2/P_1 across shock behind double-wedge areofoil and P_2/P_1 predicted from step experiments.

(60241) Wt. 17/680 K.9 2/54 Hw

PRINTED IN GREAT BRITAIN

Publications of the Aeronautical Research Council

ANNUAL TECHNICAL REPORTS OF THE AERONAUTICAL RESEARCH COUNCIL (BOUND VOLUMES)

1936 Vol. I. Aerodynamics General, Performance, Airscrews, Flutter and Spinning. 40*s.* (40*s.* 9*d.*)
Vol. II. Stability and Control, Structures, Seaplanes, Engines, etc. 50*s.* (50*s.* 10*d.*)

1937 Vol. I. Aerodynamics General, Performance, Airscrews, Flutter and Spinning. 40*s.* (40*s.* 10*d.*)
Vol. II. Stability and Control, Structures, Seaplanes, Engines, etc. 60*s.* (61*s.*)

1938 Vol. I. Aerodynamics General, Performance, Airscrews. 50*s.* (51*s.*)
Vol. II. Stability and Control, Flutter, Structures, Seaplanes, Wind Tunnels, Materials. 30*s.* (30*s.* 9*d.*)

1939 Vol. I. Aerodynamics General, Performance, Airscrews, Engines. 50*s.* (50*s.* 11*d.*)
Vol. II. Stability and Control, Flutter and Vibration, Instruments, Structures, Seaplanes, etc. 63*s.* (64*s.* 2*d.*)

1940 Aero and Hydrodynamics, Aerofoils, Airscrews, Engines, Flutter, Icing, Stability and Control, Structures, and a miscellaneous section. 50*s.* (51*s.*)

1941 Aero and Hydrodynamics, Aerofoils, Airscrews, Engines, Flutter, Stability and Control, Structures. 63*s.* (64*s.* 2*d.*)

1942 Vol. I. Aero and Hydrodynamics, Aerofoils, Airscrews, Engines. 75*s.* (76*s.* 3*d.*)
Vol. II. Noise, Parachutes, Stability and Control, Structures, Vibration, Wind Tunnels 47*s.* 6*d.* (48*s.* 5*d.*)

1943 Vol. I. (*In the press.*)
Vol. II. (*In the press.*)

ANNUAL REPORTS OF THE AERONAUTICAL RESEARCH COUNCIL—

1933–34	1*s.* 6*d.* (1*s.* 8*d.*)	1937	2*s.* (2*s.* 2*d.*)
1934–35	1*s.* 6*d.* (1*s.* 8*d.*)	1938	1*s.* 6*d.* (1*s.* 8*d.*)
April 1, 1935 to Dec. 31, 1936.	4*s.* (4*s.* 4*d.*)	1939–48	3*s.* (3*s.* 2*d.*)

INDEX TO ALL REPORTS AND MEMORANDA PUBLISHED IN THE ANNUAL TECHNICAL REPORTS, AND SEPARATELY—

April, 1950 - - - - R. & M. No. 2600. 2*s.* 6*d.* (2*s.* 7½*d.*)

AUTHOR INDEX TO ALL REPORTS AND MEMORANDA OF THE AERONAUTICAL RESEARCH COUNCIL—

1909–1949. R. & M. No. 2570. 15*s.* (15*s.* 3*d.*)

INDEXES TO THE TECHNICAL REPORTS OF THE AERONAUTICAL RESEARCH COUNCIL—

December 1, 1936 — June 30, 1939.	R. & M. No. 1850.	1*s.* 3*d.* (1*s.* 4½*d.*)
July 1, 1939 — June 30, 1945.	R. & M. No. 1950.	1*s.* (1*s.* 1½*d.*)
July 1, 1945 — June 30, 1946.	R. & M. No. 2050.	1*s.* (1*s.* 1½*d.*)
July 1, 1946 — December 31, 1946.	R. & M. No. 2150.	1*s.* 3*d.* (1*s.* 4½*d.*)
January 1, 1947 — June 30, 1947.	R. & M. No. 2250.	1*s.* 3*d.* (1*s.* 4½*d.*)
July, 1951.	R. & M. No. 2350.	1*s.* 9*d.* (1*s.* 10½*d.*)

Prices in brackets include postage.

Obtainable from

HER MAJESTY'S STATIONERY OFFICE

York House, Kingsway, London, W.C.2; 423 Oxford Street, London, W.1 (Post Orders: P.O. Box 569, London, S.E.1); 13a Castle Street, Edinburgh 2; 39, King Street, Manchester, 2; 2 Edmund Street, Birmingham 3; 1 St. Andrew's Crescent, Cardiff; Tower Lane, Bristol 1; 80 Chichester Street, Belfast, or through any bookseller

S.O. Code No. 23–2800